

Low global-warming-potential refrigerant CH₂F₂ (R-32): Integration of a radiation heat loss correction method to accurately determine experimental flame speed metrics

Raik Hesse^{a,*}, Lukas Berger^a, Chaimae Bariki^a, Michael J. Hegetschweiler^b, Gregory T. Linteris^b, Heinz Pitsch^a, Joachim Beeckmann^a

^a*Institute for Combustion Technology, RWTH Aachen University, 52056 Aachen, Germany*

^b*Energy and Environment Division, National Institute of Standards and Technology, Gaithersburg, MD 20899, USA* **

Abstract

Due to their high global warming potential (GWP), hydrofluorocarbon refrigerants are systematically being phased out. Replacements with low GWP exist, but give rise to safety hazards as they are found to be mildly flammable. The assessment of the safety hazards of such fluids is typically based on their laminar flame speed. Typical laminar flame speeds are below 10 cm/s, and hence are challenging to measure. Flames propagating at this speed are strongly affected by radiation heat loss and have to be corrected if considered for kinetic model validation. In the present study, the laminar flame speed of the representative refrigerant difluoromethane (CH₂F₂, R-32) is measured experimentally in an outwardly propagating flame configuration at elevated pressure and temperature. To assess radiation heat loss effects, detailed simulations using a recent kinetic model for CH₂F₂ are conducted. Flame speed reductions due to radiation are found to be in the order of 15 %. An analytical radiation correction model, as discussed by Santner et al. [Combust. Flame, 161(1), (2014), 147-153.], is adopted and its suitability for refrigerant/air flames is demonstrated based on simulation. After subsequent correction of experimental results, the predictability of the model is evaluated, showing good agreement.

Keywords:

Difluoromethane, Refrigerant, Laminar Flame Speed, Spherical Propagating Flame, Fire Safety, Radiation

** Official contribution of NIST, not subject to copyright in the United States. Certain commercial equipment, instruments, and materials are identified in this paper to adequately specify procedure. Such identification does not imply recommendation or endorsement by the National Institute of Standards and Technology.

*Corresponding author:

Email address: r.hesse@itv.rwth-aachen.de (Raik Hesse)

1. Introduction

The contribution of hydrofluorocarbon (HFC) based refrigerants on the total radiative forcing of the Earth is projected to be large [1]. Increasing the hydrogen substitution and the use of unsaturated HFCs (alkenes) are viable solutions to increase the reactivity and thus decomposition in the troposphere, with the drawback of promoting flammability. The laminar flame speed, S_L , is typically used to assess the flammability of fuel/oxidizer mixtures. S_L provides information on the overall reactivity and can be used to constrain uncertainties of chemical models or as a scaling factor in turbulent combustion models [2]. Several different measurement techniques have been introduced to measure laminar flame speeds of refrigerant flames, e.g. the nozzle burner [3], the tube method [4, 5], the constant volume method [6, 7], and the outwardly propagating flame method (OPF) measured under quasi-isobaric conditions [8, 9].

In this paper, the discussion exclusively refers to spherical expanding flame experiments using the Schlieren method unless otherwise stated. This method has been favored because of its closed measurement environment and the well-defined boundary conditions. Harmful combustion residues, such as hydrogen fluoride, can be neutralized internally without decontamination of the laboratory environment. Recently, great attention has been paid to improve the robustness of OPF measurements of conventional hydrocarbons by assessing their uncertainties associated with S_L , including strategies to reduce these [10–14]. However, flame speed studies on refrigerants are rare, and the techniques to quantify uncertainties are not proven to be fully applicable for HFCs.

This all leads to the necessity to extend experimental data on the flammability of refrigerants, which is the objective of the present study. For this, difluoromethane (CH_2F_2 , R-32) has been chosen as a representative refrigerant. CH_2F_2 was subject of previous flame speed studies, mostly at atmospheric conditions [4, 6, 8] or using a non-optical measurement method [7, 15].

In order to use the experimental data for kinetic model validation, uncertainty sources have to be well-estimated. Uncertainties due to radiation heat loss originate from the slow burning velocities of refrigerants like CH_2F_2 . Flame speeds of these are almost one order of magnitude lower than those of typical hydrocarbons, such as methane and n-heptane. Besides, slow burning flames can be affected by buoyancy and stretch, which are discussed elsewhere (e.g., [16]) and are not subject of the present study. Measurement conditions have been

carefully chosen to impede these effects.

Radiation effects on S_L are reportedly much higher for HFCs than for hydrocarbons [7]. Radiation is always present in spherical flame experiments and is most prominent for slowly propagating flames, as the case for HFCs. Thus, derived S_L are inherently depressed and cannot readily be used for kinetic model validation. However, in most experimental studies on refrigerant/air flames the effect of radiation has been neglected. Uncertainties in radiation are typically addressed in terms of a worst case estimation using simulations of spherically expanding flames under adiabatic conditions and with the optically thin radiation model (OTM) [17, 18]. The OTM does not consider absorption of the emitted radiation and can result in large overestimations of the radiation effect, as has been discussed for flames in CO_2 dilution by Chen [13]. In these cases, a statistical narrow-band model (SNB) provides more accurate predictions. [19]. However, reaction kinetic computations incorporating a SNB model are quite expensive and require a reliable kinetic model. Neither a suitable kinetic model nor the necessary SNB-parameters for species involved in refrigerant combustion might be available prior to an experimental study.

Yu et al. [20] proposed an empirical correlation approach, which can be easily adopted for hydrocarbon OPFs. The model has been validated for flame speeds faster than 10 cm/s, but HFC refrigerants typically involve flame speeds below 10 cm/s, which remain unconsidered in the Yu et al. model. For hydrogen and n-heptane flames, Santner et al. [18] proposed a correction based on a thermodynamic calculation to correct for radiation. This approach estimates the thermal and flow effects caused by radiation separately.

The goal of the present work is to extend Santner's correction approach for slow-burning CH_2F_2 /air flames and expand the database of robustly measured flame speeds for kinetic modeling studies. For fire safety concerns, the flame behavior, kinetic model performance, and experimental measurements obtained with normal air is of most interest. To maintain a slow flame speed, standard combustion air has been chosen instead of O_2 -enriched air.

The paper is structured as follows: First, flames are simulated to assess the effect of radiation on a slowly propagating flame and to examine the applicability of the approach by Santner et al. [18] for CH_2F_2 . Second, measurements are conducted in a spherical combustion chamber, with the purpose of extending the database on CH_2F_2 to elevated pressures and temperatures. Finally, the analytical scheme is applied to experiments and the validity of a recent kinetic model by Burgess et al. [21]

is discussed.

2. Experimental framework

2.1. Apparatus and procedures

Flame speed measurements were conducted using the closed-vessel method combined with an optical Schlieren cinematography setup comparable to the setup described by Beeckmann et al. [22]. The setup, illustrated in Fig. 1, consists of a spherical combustion chamber with an inner diameter of 119.8 mm. The chamber is optically accessible via two 50 mm diameter cylindrical windows on opposite sites. To increase the resistance of the windows to hydrogen fluoride, which is a product of the combustion of refrigerants, sapphire crystal has been chosen as window material. A dual-field-lens Schlieren arrangement, as described in [23], was installed together with a high-power LED emitting red light. Images were recorded at 5,000 frames per second (fps) with a high-speed CMOS camera, type Photron Fastcam. The suitability of the camera regarding the image resolution was checked by artificially reducing the pixel ratio until the post-processed data gets affected. The image size of 384×384 pixels at a resolution of 8.47 pixel/mm was found to be sufficiently above this threshold, also illustrated in Fig. S2 of the Supplementary material. The accuracy of flame speed experiments substantially depends on the mixture preparation. Here, high accuracy Alicat mass flow controllers (MFC) were used supplying combustion air and refrigerant, at 5 and 1 slpm, respectively. MFC uncertainties can be estimated to 0.4 % of the reading and 0.2 % of the full-scale, which results in a maximum uncertainty in equivalence ratio of 2.5 %. The combustion air is compressed, filtered, and dehumidified (< 0.01 ppm) ambient air, with volume fractions of 20.94 % oxygen, 78.13 % nitrogen, and 0.93 % argon. CH₂F₂ with 99.5 % purity was sourced from Westfalen gas. First, the entire tube system is evacuated several times to remove residual gases and then flushed with premixed refrigerant/air mixture. Initial pressures can be varied by adjusting a needle valve in the outlet of the combustion chamber until the pressure has reached a stationary level. Then the chamber inlet and outlet valves are closed at once. After an appropriate settling time of 5 min, the mixture is centrally ignited by a two-step coil and capacitor ignition system, providing spark energies up to 5 J. However, for most of the conditions, energies are below 500 mJ. The spark is discharged via extended spark plug electrodes with a diameter of 1 mm. The gap between both electrodes is 2 mm. Ignition energies were

gradually increased in order to reduce the effect of ignition energy on the flame evolution. The combustion pressure is measured via an absolute Kistler pressure transducer of type 4075A50 with a measurement uncertainty of 0.15 %. The combustion chamber and its periphery can be heated for measurements at elevated temperatures.

New measurements of CH₂F₂/air mixtures were carried out at 333 K for pressures of 2 bar and 3 bar and equivalence ratios ranging from 0.9 to 1.6.

2.2. Determination of flame speeds

Flame front extraction is restricted to spherically smooth flame fronts above a critical radius associated with the complete decay of ignition effects and within a quasi-isobaric regime allowing for a pressure rise of maximum 2 % [24, 25]. Schlieren images are background-subtracted and the flame front is extracted using the method of Otsu et al. [26]. Thus, the temporal evolution of the flame radius R_f can be obtained at its temperature iso-surface. For Schlieren photography of spherically expanding flames this threshold is at 840 K [27]. Applying a central differences scheme yields the stretched propagation speed with respect to the burned mixture $s_b = dR_f/dt$. The stretch rate κ of an outwardly propagating flame is defined as the temporal change of the flame surface area A leading to $\kappa = 1/A \cdot dA/dt = 2/R_f \cdot dR_f/dt$ [28]. The linear relation between flame stretch and the flame propagation speed

$$s_b^0 - s_b = \mathcal{L}_b \kappa \quad (1)$$

is well known. \mathcal{L}_b represents the Markstein number in the burned gas. [29, 30] A least square fitting scheme yields s_b^0 and \mathcal{L}_b . Through the years, other extrapolation schemes have been discussed addressing the non-linearity in experimentally obtained propagation speeds, especially in the negative Markstein length regime and at highly stretched flames. The different methods have been bench-marked with respect to their extrapolation uncertainties by Kelley et al. [31] and by Wu et al. [32]. Kelley et al. provided an analytical expression in dimensional form yielding

$$s_b^0 t + c = R_f + 2\mathcal{L}_b \ln R_f - 4 \frac{\mathcal{L}_b^2}{R_f} - \frac{8}{3} \frac{\mathcal{L}_b^3}{R_f^2}. \quad (2)$$

The variable c is an integration constant. This method was found to be robust and easy to handle in a numerical regression least square fitting scheme of the experimental flame radii and the corresponding time [31]. An exemplary flame evolution of CH₂F₂/air flames at

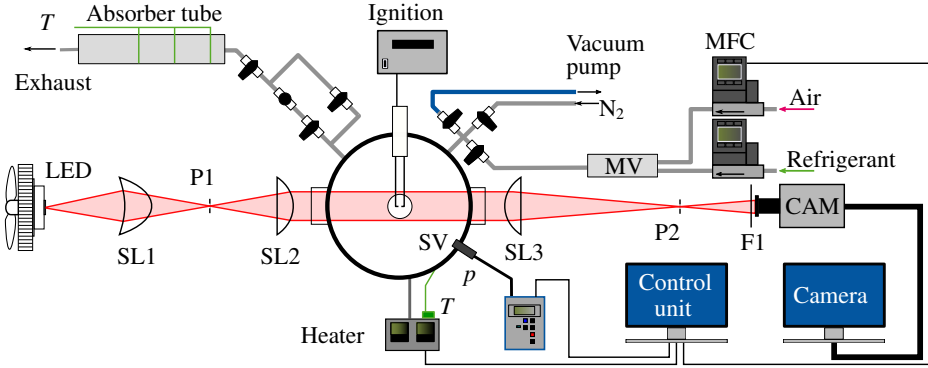


Figure 1: Sketch of the experimental setup. Abbreviations, SL1, 2, and 3 refer to the spherical lenses utilized in the Schlieren arrangement. P1 and P2 are pinholes. F1 denotes the filter used to prevent the camera from overexposure due to the flame luminescence. MV refers to the mixing vessel downstream of the Mass flow controllers (MFC).

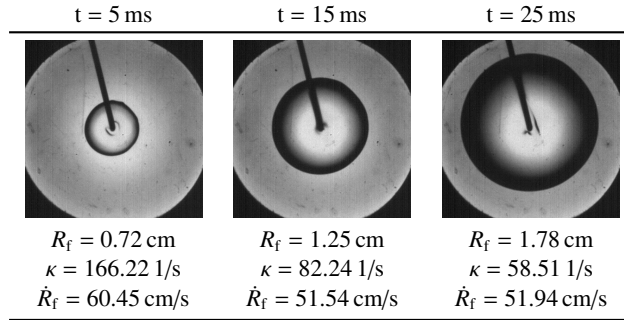


Figure 2: Raw flame recordings of $\text{CH}_2\text{F}_2/\text{air}$ mixtures at $\phi = 1.1$, $T = 298 \text{ K}$ and 3 bar at 5, 15, and 25 ms after ignition.

$\phi = 1.1$ and $T = 298 \text{ K}$ is shown in Fig. 2. In the present work, the center of the flame and its outer contour are tracked for the flame evolution yielding no evidence of buoyancy-induced distortion or intrinsic instabilities. This can also be seen in Figs. S3 to S5 of the Supplementary material. The unstretched flame speed, S_L , can be evaluated for adiabatic flames by mass continuity through a planar unstretched flame, $S_L = s_u^0 = s_b^0(\rho_b/\rho_u)$, where ρ_b and ρ_u are the burned and unburned densities, respectively. It will be later shown that this method does not hold true, since the burned gas velocity is neglected for symmetry reasons, which is not a suitable assumption in the presence of radiation heat loss.

3. Numerical framework

3.1. Flame speed calculation

Flame speed simulations of planar stationary flames and spherically propagating transient flames were performed using the appropriate modules of the open-source code FlameMaster [33]. For the calculation of

spherically expanding flames, the set of conservation equations in one-dimensional geometries is described by Maas and Warnatz [34]. Zero gradient outflow conditions preserve isobaric conditions during flame growth. Ignition is initiated by enthalpy increase, which mimics a realistic ignition behavior. Gradients are properly resolved using a dynamic grid refinement algorithm. At least 20 gridpoints are used to resolve the flame thickness. For verification, unstretched flame speeds s_b^0 of the stationary and transient planar configuration were compared, yielding good agreement.

3.2. Chemical kinetic mechanism

CH_2F_2 flames are modeled using a recently developed chemical kinetic mechanism by Burgess et al. [21] containing 101 species and 420 elementary reactions. Here, a reduced version of this mechanism has been used to decrease computational time for transient simulations. Unstretched, premixed flame simulations using the reduced model incorporating 28 species and 94 reactions were compared to the full mechanism showing no significant differences. Radiation effects were modeled for species in the burned equilibrated gas, CO_2 , CO , H_2O , and HF , using the optically thin model, thus assuming the absence of radiation absorption. Modeling the latter using more complex SNB models is currently unfeasible due to the fact that SNB model parameters of some major species involved in refrigerant combustion are missing.

4. Results and discussion

Figure 3 depicts the experimentally measured propagation speed of two exemplary $\text{CH}_2\text{F}_2/\text{air}$ flames with

an equivalence ratio of $\phi = 1.1$ and $\phi = 1.5$ at 3 bar and 333 K. The **extrapolated, unstretched laminar flame speeds** are low so that they are most likely affected by radiation heat loss, as suggested by several studies [18, 20]. Standard post-processing of the data and assuming adiabatic conditions can no longer be performed. This raises the question, how these flames can be corrected to account for the **effect** of radiation heat loss. Radiation heat loss affects the flame in two ways. First, it induces a kinematic effect as it reduces the **burned** gas temperature, which results in an inward flow towards the cooling core of the burned gas region and **a reduction of the flame's expansion velocity**. Secondly, radiation affects the interplay of chemistry and diffusion within the flame front, since the temperature gradient in the burned gas causes conductive heat loss from the reaction zone to the cooling center of the flame. Additionally, radiation heat is emitted from the flame zone into the unburned gas mixture. Both heat losses decrease the flame temperature, which has a significant effect on flame speed.

Therefore, three error sources can be identified: 1. Extrapolated flame speeds are reduced by the inward gas motion (kinematic effect); 2. Underestimation of S_L due to false density assumptions for the burned gas; 3. Extrapolation errors due to the nonlinear relationship between the propagation speed and stretch rate.

The **third** error can be suppressed by increasing initial pressures, **as discussed by Wu et al. [32]**. However, **in very lean $\text{CH}_2\text{F}_2/\text{air}$ mixtures, the involved nonlinear dependence on the stretch rate caused by the non-equidiffusion of heat and mass characterized by non-unity Lewis numbers is significant**. This effect also causes an increase in the critical flame initiation radius with the requirement for larger ignition energy deposits [24]. This significantly reduces the available data range for extrapolation to zero stretch of lean $\text{CH}_2\text{F}_2/\text{air}$ flames yielding higher uncertainties of the extrapolation scheme. Hence, these flames were omitted by restricting the following analysis to conditions with equivalence ratios larger than 1.05 at an initial pressure of 2 bar. For higher pressures, this condition could be relaxed, including also lean cases.

The first two **errors** are discussed in the following. Unfortunately, radiation heat loss cannot be **directly** measured experimentally in spherically expanding flames **due to the lack of high-speed and high-resolution radiometers**. The approach proposed in this study is based on an analytically derived model to account for radiation heat losses by Santner et al. [18]. This approach has been validated for cases of hydrogen and n-heptane flames. As a first step, the applicability of

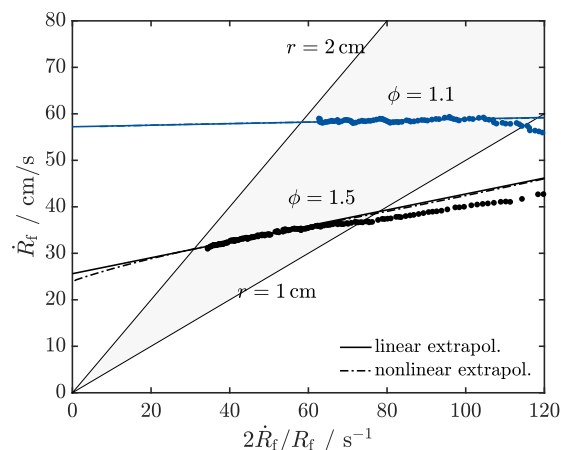


Figure 3: Propagation speed against the stretch rate for two sample $\text{CH}_2\text{F}_2/\text{air}$ flames at $\phi = 1.1$ and $\phi = 1.5$, both at 3 bar and 333 K.

this approach for CH_2F_2 cases is shown. Detailed OPF simulations of $\text{CH}_2\text{F}_2/\text{air}$ mixtures serve as a reference case, and the predictability of the model is discussed. It is subsequently adopted for the new experimental data obtained in the present study.

4.1. Adoption of the analytical scheme

The analytical model by Santner et al. [18] can be subdivided into several steps:

1. modeling the burned temperature over the radius,
2. deriving the burned gas velocity u_b from mass conservation,
3. correction of the propagation speed,
4. modeling the heat fluxes for heat conduction and radiation from the flame zone,
5. and deriving the effect of radiation due to the heat fluxes.

Here, the basic steps are presented **based on** a representative stoichiometric case for $\text{CH}_2\text{F}_2/\text{air}$ at 3 bar and 333 K. The corresponding propagation speeds as a function of stretch are plotted in Fig. 4. At first, only the **transient 1D simulations are** considered, which are labeled $s_{b,ADI}$ (upward triangle) and $\dot{R}_{f,OTM}$ (square), depicting the adiabatic and OTM simulations. Note that the propagation speed in the OTM case is not an s_b in the traditional sense, because it is affected by radiation heat loss, and therefore it is denoted as $\dot{R}_{f,OTM}$. **For the adiabatic case, the propagation speed grows linearly with decreasing stretch rate**. In contrast, a strong nonlinear behavior can be noticed for the OTM. **There are several reasons why the propagation speed over the stretch rate of a spherical flame can become nonlinear**. One

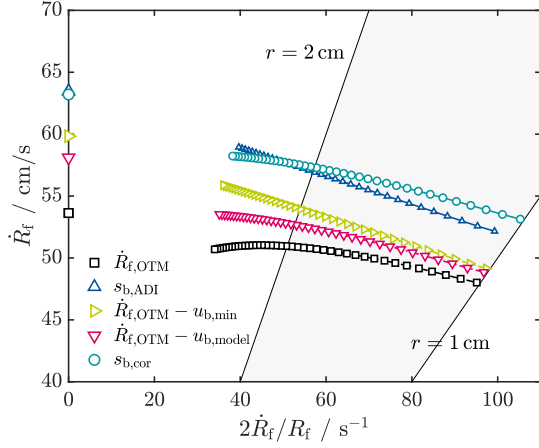


Figure 4: Simulated and corrected propagation speeds of a $\text{CH}_2\text{F}_2/\text{air}$ flame at $\phi = 1.0$, $p_u = 3$ bar, and $T = 333$ K. The gray background area depicts the radii evaluation range of 1 to 2 cm.

is the impact of radiation heat loss. Another reason is the pressure rise due to confinement effects. The latter was eliminated by restricting the data range to a maximum pressure rise of 2 %. At small radii, meaning high stretch rates, the propagation speed $\dot{R}_{f,\text{OTM}}$ progresses in the same manner as the adiabatic case, however, at significantly lower propagation speed. Unstretched propagation speeds were determined using the linear extrapolation scheme, depicted as symbols on the ordinate axis. Due to the non-linearity of the radiation case, extrapolation involves large errors. This underlines the need for an appropriate correction method. The experimental framework was matched by selecting a data range of 1 to 2 cm for extrapolation. It can be seen that interpreting the results from the OTM simulation as adiabatic, yields large deviations for s_b^0 of about 15 %. Data with such large errors cannot be used in the context of kinetic mechanism validation. Next, the OTM simulation is corrected by subtracting the burned gas velocity u_b from the propagation speed, so that s_b is equal to $\dot{R}_f - u_b$. The flame is assumed to be thin so that a discontinuity jump can describe the temperature and velocity over the flame front. Thus, the minimum burned gas velocity $u_{b,\text{min}}$ can be interpreted as u_b , yielding the corrected propagation speed $\dot{R}_f - u_{b,\text{min}}$ in Fig. 4 (right pointed triangle). As for the adiabatic case, a linear increase in the propagation speed with the same Markstein length can be observed. Now, u_b is determined using the analytical model as proposed by Santner et al. [18]. At first, a formulation for u_b depending on the burned gas temperature is derived from mass continuity. The ideal gas law is substituted assuming a constant molecular weight, a spatially averaged temperature of the burned gas \bar{T}_b , and

the adiabatic flame temperature T_{ad} at the flame radius R_f yields

$$u_b = \frac{R_f}{3} \frac{T_{\text{ad}}}{\bar{T}_b^2} \frac{d\bar{T}_b}{dt}. \quad (3)$$

A simplified model of the burned temperature over radius $T(r)$ is derived from the governing equations for energy and mass conservation assuming frozen chemistry of the burned gas. Thus, viscous heating and mass diffusion can be neglected. In addition, the convection and conduction term were found to be significantly smaller than unity and can be neglected as well, so that

$$\rho c_p \frac{\partial T}{\partial t} = q_r = -4\sigma K_p P (T^4 - T_u^4). \quad (4)$$

σ is the Stefan-Boltzmann constant and p the pressure. With $T^4 \gg T_u^4$, the Planck mean absorption coefficient K_p assumed to be constant in the burned core of the flame, and the conversion to spatial coordinates using $t = (R_f - r)/\dot{R}_f$, $T(r)$ can be written as

$$T(r) = T_{\text{ad}} \left(\alpha \left(\frac{R_f - r}{R_f} \right) + 1 \right)^{-\frac{1}{4}}. \quad (5)$$

In this context, \dot{R}_f is assumed as constant. α , the composite radiation parameter, describes the temperature decay rate due to radiation heat loss

$$\alpha = \frac{16\sigma K_p \mathcal{R} T_{\text{ad}}^4}{c_p}, \quad (6)$$

with the universal gas constant \mathcal{R} . Constant temperature in the burnt gas has been assumed for the molar heat c_p at equilibrium, which is evaluated from NASA polynomials. By spatial integration of $T(r)$ over $0 < r < R_f$, the spatially averaged burned temperature is deduced

$$\bar{T}_b(R_f) = T_{\text{ad}} \left(1 - \frac{\alpha R_f}{16\dot{R}_f} \right). \quad (7)$$

Including \bar{T}_b in Eq. 3 and replacing $2\dot{R}_f/R_f$ with the stretch rate κ yields the burned gas velocity

$$u_b = -\frac{\alpha \dot{R}_f}{24} \left(\frac{1}{\kappa} + \frac{\alpha}{4\kappa^2} \right). \quad (8)$$

Model parameters are summarized in Tab. 1. By correcting $\dot{R}_{f,\text{OTM}}$ in Fig. 4 with $u_{b,\text{model}}$ (downward triangle) the propagation speed increases. Whereas the model predicts very similar propagation speeds at small radii, it deviates from the detailed solution for larger

Table 1: Summary of model parameters at $p_u = 3$ bar and $T_u = 333$ K.

ϕ	T_{ad}	ρ_u	ρ_b	l_f	K_p	c_p/\mathcal{R}	α	u_b^0	s_b^0	λ/c_p	T_a	$S_{L,ADI}/S_{L,cor}$
-	K	kg/m ³	kg/m ³	mm	atm ⁻¹ /m ⁻¹	-	1/s	cm/s	cm/s	g/ms	K	-
0.9	2159	3.52	0.468	0.559	0.7818	4.70	32.33	-3.67	51.87	0.103	37518	0.97
1.0	2235	3.56	0.450	0.5132	0.7679	4.75	36.15	-3.92	62.25	0.106	44422	1.00
1.1	2215	3.60	0.448	0.4944	0.7207	4.68	33.22	-3.47	62.58	0.105	35752	0.97
1.3	2067	3.66	0.467	0.5587	0.7426	4.53	26.76	-2.59	50.13	0.100	35362	0.98
1.5	1927	3.73	0.488	0.8075	0.7790	4.40	21.86	-2.11	33.14	0.095	37052	1.01

flames. Applying the typical extrapolation range of 1 to 2 cm yields deviations in \dot{R}_f^0 of about 3 %.

The propagation speed, analytically corrected for u_b , still needs to be adjusted for the conductive and radiation heat loss of the flame zone. Santner et al. [18] provide an extrapolation methodology to account for radiation effects, given as

$$\frac{S}{S^0} \ln\left(\frac{S}{S^0}\right) = -\frac{T_a \lambda \alpha}{8T_{ad} c_p \rho_b (\dot{R}_f^0)^2} \cdot \left[\frac{7}{6} + \frac{2T_u}{15T_{ad}} + O\left(\left(\frac{T_u}{T_{ad}}\right)^2 \dots\right) \right]. \quad (9)$$

S/S^0 is the flame speed reduction caused by the flame temperature reduction. Typically, \dot{R}_f^0 is the experimentally measured and extrapolated propagation speed to zero stretch. Heat conductivity and molar heat are evaluated from the approximation by Smooke [35]¹. T_a is the activation temperature [36], which is given as

$$T_a = -2 \left(\frac{\partial \ln(\rho_u S_L)}{\partial (1/T_f)} \right)_p \quad (10)$$

and is gained from perturbation of the unburned temperature in unstretched premixed simulations or from experiments by varying the initial temperature.

So far, both effects, the inward gas motion and the decrease of the flame temperature, were derived separately. By combining both, $s_{b,cor}$ is determined and represented by circles in Fig. 4. It can be seen that extrapolated unstretched propagation speeds, using the 1 to 2 cm data range, are very comparable. However, the stretch dependence of the adiabatic and the corrected propagation speeds are slightly different. The nonlinear effect in the corrected flame evolution is caused by slight underprediction of the burned gas temperature.

By multiplying with the density ratio of the adiabatic, case the unstretched propagation speeds obtained after

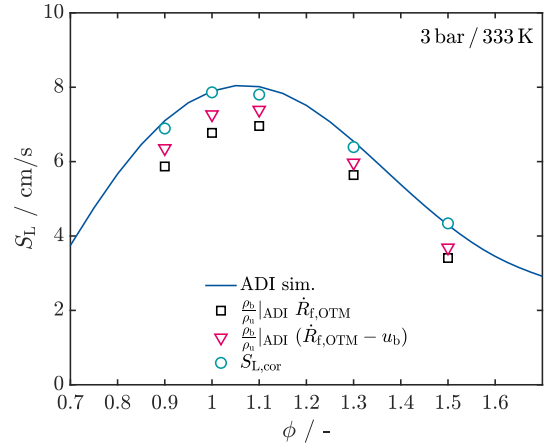


Figure 5: Detailed simulation of laminar burning velocities of $\text{CH}_2\text{F}_2/\text{air}$ mixtures at 3 bar and 333 K and corrected propagation speed using the analytical model by Santner et al. [18].

extrapolation are converted to burning velocities with respect to the unburned gas. In Fig. 5, laminar burning velocities of the detailed simulations are shown over the equivalence ratio. The solid line represents the results from adiabatic unstretched premixed simulation. Symbols represent the extrapolated values obtained from the transient simulation for the OTM (squares), u_b -corrected propagation speeds (triangles), and after total correction $S_{L,cor}$ (circles). The corrected laminar flame speeds agree well with the adiabatic simulation within an error of less than 3 %. As can also be seen in Eq. 8, the burned gas velocity strongly scales with the propagation speed, since α does not change significantly. A constant reduction in flame speed caused by u_b of 7 % can be observed. The flame zone cooling effect scales with $1/(\dot{R}_f^0)^2$ (Eq. 9), and therefore is of much higher importance at rich conditions, where the flame speeds are low. The total radiation-induced flame speed reduction is about 15 % for equivalence ratios ranging from 1.0 to 1.3. At lean and rich conditions, radiation effects become larger and yield 17 % and 21 % decreased flame

¹ $\frac{\lambda}{c_p} = 2.58 \times 10^{-4} \frac{\text{g}}{\text{cm s}} \left(\frac{T}{298\text{K}} \right)^{0.7}$

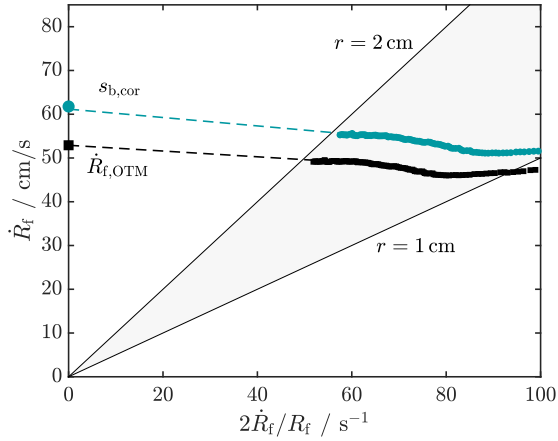


Figure 6: The experimentally measured and the corresponding radiation corrected propagation speed of a $\text{CH}_2\text{F}_2/\text{air}$ flame at $\phi = 1.0$, $p_u = 3$ bar, and $T = 333$ K.

speeds, respectively. The remaining modeling error of 3 % was estimated in the 1 to 2 cm radii regime, and will most certainly increase if larger flames are evaluated. Combining the findings from the analysis of detailed simulations with the experimental uncertainty yields an overall uncertainty of < 5 %, which is a significant improvement considering the large influence of radiation heat loss on the flame speed up to 21 %. However, one should not forget that involving the OTM could result in an overcorrection. The radiation absorption behavior of fluorinated refrigerants has to be discussed in future studies.

4.2. Radiation-corrected experiments

In the previous section, the analytical model by Santner et al. [18] was tested for its applicability to $\text{CH}_2\text{F}_2/\text{air}$ flames based on detailed simulations. A good agreement was observed for the laminar flame speed. This encourages the application of the analytical radiation correction scheme to experimental data. In Fig. 6, the original and corrected propagation speeds are shown for a stoichiometric $\text{CH}_2\text{F}_2/\text{air}$ flame at 3 bar and 333 K, complementary to the exemplary simulation case from Fig. 4. Extrapolations were performed in the non-ignition-affected range, which starts slightly above a flame radius of 1 cm. Other data points have been evaluated accordingly. The corrected and extrapolated propagation speeds are not shown in the present work for reasons of clarity. Instead, laminar burning velocities are presented in Fig. 7 and compared to those calculated for 1D, planar, adiabatic flames using the kinetic mechanism by Burgess et al. [21]. The original experimental data (squares), assuming the adiabatic limit, are

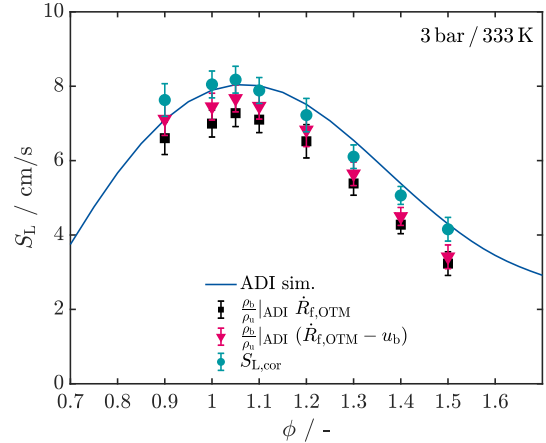


Figure 7: Uncorrected and radiation-corrected experimental laminar flame speed over equivalence ratio of $\text{CH}_2\text{F}_2/\text{air}$ flames at 3 bar and 333 K.

not comparable to the chemical kinetic model (line), due to the large errors caused by radiation heat loss. Only after correction, the data can be considered as validation targets. The model shows good agreement over the entire range of equivalence ratios and predicts the peak velocity, located at $\phi = 1.05$ with good accuracy. For reasons of completeness, results for 2 bar and 333 K are shown in Fig. S8 of the Supplementary material. Flame speed results at $\phi = 0.9$ and $\phi = 1.0$ are not included, since at these conditions a strong nonlinear evolution of \dot{R}_f has been observed yielding too large errors when extrapolating to the unstretched values. As for the 3 bar case, the kinetic model shows good agreement. In experiments, a peak velocity of 8.94 cm/s and 8.18 cm/s is derived for 2 bar and 3 bar, respectively.

5. Concluding remarks

Laminar burning velocities of $\text{CH}_2\text{F}_2/\text{air}$ have been investigated experimentally using the OPF method. Conditions were chosen at elevated temperatures and pressures for a broad range of equivalence ratios ranging from 0.9 to 1.6. The increase in pressure decreased the nonlinearity in the flame evolution of the propagation speed so that more accurate data could be measured. Due to the low burning velocities, below 10 cm/s, experimental results are expected to be influenced by radiation heat loss, which must be considered to obtain reliable flame metrics. Transient 1D simulations of OPFs were conducted for the adiabatic and OTM limit using a recent CH_2F_2 kinetic model [21]. The simulations revealed strong radiation-induced thermal and flow effects for all $\text{CH}_2\text{F}_2/\text{air}$ flames, which reduce the flame speed

by 15 % to 21 %. An analytical solution to assess radiation effects in flames proposed by Santner et al.[18] was adopted for CH₂F₂ and verified using simulations employing a detailed chemical mechanism. Overall good agreement has been observed, highlighting the suitability of this approach for correction of radiation-affected experimental data from CH₂F₂. After considering the OTM limit for the experimental data and correcting it with the tested approach, a corrected laminar flame speed was determined. The kinetic model showed excellent agreement with the radiation-corrected experimental data. The peak flame speed of CH₂F₂ at 3 bar and 333 K yields 8.18 cm/s at $\phi = 1.05$. Further investigations of the applicability for even slower refrigerants, such as R-1234yf, will be conducted in the future.

Acknowledgments

The authors from RWTH Aachen University gratefully acknowledge the generous support of the National Institute of Standards and Technology, U. S. Department of Commerce, (Grant No. 70NANB17H276). The work at NIST was supported by the Buildings Technologies Office of the U.S. Department of Energy, Office of Energy Efficiency and Renewable Energy under contract no. DE-EE0007615 with Antonio Bouza serving as Project Manager.

References

- [1] G. J. Velders, A. R. Ravishankara, M. K. Miller, M. J. Molina, J. Alcamo, J. S. Daniel, D. W. Fahey, S. A. Montzka, S. Reimann, Preserving Montreal Protocol climate benefits by limiting HFCs, *Science* 335 (2012) 922–923.
- [2] N. Peters, *Turbulent Combustion*, Cambridge University Press, 2000. Cambridge Books Online.
- [3] G. T. Linteris, Burning velocity of 1, 1-difluoroethane (r-152a), *ASHRAE Transactions* 112 (2006) 448.
- [4] D. Clodic, T. Jabbour, Method of test for burning velocity measurement of flammable gases and results, *HVAC&R Research* (2011).
- [5] P. Papas, S. Zhang, W. Kim, S. Zeppieri, M. Colket, P. Verma, Laminar flame speeds of 2,3,3,3-tetrafluoropropene mixtures, *Proc. Combust. Inst.* (2016).
- [6] K. Takizawa, A. Takahashi, K. Tokuhashi, S. Kondo, A. Sekiya, Burning velocity measurement of fluorinated compounds by the spherical-vessel method, *Combust. Flame* 141 (2005) 298 – 307.
- [7] R. R. Burrell, J. L. Pagliaro, G. T. Linteris, Effects of stretch and thermal radiation on difluoromethane/air burning velocity measurements in constant volume spherically expanding flames, *Proc. Combust. Inst.* 37 (2019) 4231 – 4238.
- [8] S. Takagi, K. Tokuhashi, Assessment of burning velocity test methods for mildly flammable refrigerants, part 1: Closed-vessel method, *ASHRAE Transactions* 119 (2013) 243.
- [9] B. Choi, J. Park, A. Ghoniem, Characteristics of outwardly propagating spherical flames of R134a (C2H2F4)/CH₄/O₂/N₂ mixtures in a constant volume combustion chamber, *Energy* 95 (2016) 517 – 527.
- [10] F. Egolfopoulos, N. Hansen, Y. Ju, K. Kohse-Höinghaus, C. Law, F. Qi, Advances and challenges in laminar flame experiments and implications for combustion chemistry, *Prog. Energy Combust. Sci.* 43 (2014) 36–67.
- [11] Y. Chen, R. Raine, A study on the influence of burning rate on engine knock from empirical data and simulation, *Combust. Flame* 162 (2015) 2108–2118.
- [12] C. Xiouris, T. Ye, J. Jayachandran, F. Egolfopoulos, Laminar flame speeds under engine-relevant conditions: Uncertainty quantification and minimization in spherically expanding flame experiments, *Combust. Flame* 163 (2016) 270–283.
- [13] Z. Chen, Effects of radiation on large-scale spherical flame propagation, *Combust. Flame* 183 (2017) 66 – 74.
- [14] J. Beeckmann, R. Hesse, J. Schaback, H. Pitsch, E. Varea, N. Chaumeix, Flame propagation speed and markstein length of spherically expanding flames - assessment of extrapolation and measurement techniques, *Proc. Combust. Inst.* 37 (2019) 1521–1528.
- [15] A. Moghaddas, C. Bennett, E. Rokni, H. Metghalchi, Laminar burning speeds and flame structures of mixtures of difluoromethane (HFC-32) and 1,1-difluoroethane (HFC-152a) with air at elevated temperatures and pressures, *HVAC&R Research* (2014).
- [16] L. Berger, R. Hesse, K. Kleinheinz, M. J. Hegetschweiler, A. Attili, J. Beeckmann, G. T. Linteris, H. Pitsch, A DNS study of the impact of gravity on spherically expanding laminar premixed flames, *Combust. Flame* 216 (2020) 412 – 425.
- [17] J. Jayachandran, R. Zhao, F. Egolfopoulos, Determination of laminar flame speeds using stagnation and spherically expanding flames: Molecular transport and radiation effects, *Combust. Flame* 161 (2014) 2305–2316.
- [18] J. Santner, F. Haas, Y. Ju, F. Dryer, Uncertainties in interpretation of high pressure spherical flame propagation rates due to thermal radiation, *Combust. Flame* 161 (2014) 147–153.
- [19] Z. Chen, X. Qin, B. Xu, Y. Ju, F. Liu, Studies of radiation absorption on flame speed and flammability limit of CO₂ diluted methane flames at elevated pressures, *Proc. Combust. Inst.* (2007).
- [20] H. Yu, W. Han, J. Santner, X. Gou, C. H. Sohn, Y. Ju, Z. Chen, Radiation-induced uncertainty in laminar flame speed measured from propagating spherical flames, *Combust. Flame* 161 (2014) 2815–2824.
- [21] D. R. Burgess, J. A. Manion, R. R. Burrell, V. I. Babushok, M. J. Hegetschweiler, G. T. Linteris, in: 11th U. S. National Combustion Meeting Organized by the Western States Section of the Combustion Institute.
- [22] J. Beeckmann, L. Cai, H. Pitsch, Experimental investigation of the laminar burning velocities of methanol, ethanol, n-propanol, and n-butanol at high pressure, *Fuel* 117, Part A (2014) 340–350.
- [23] G. Settles, *Schlieren and Shadowgraph Techniques: Visualizing Phenomena in Transparent Media*, volume 2, Springer Berlin, 2001.
- [24] Z. Chen, M. Burke, Y. Ju, Effects of Lewis number and ignition energy on the determination of laminar flame speed using propagating spherical flames, *Proc. Combust. Inst.* 32 (2009) 1253–1260.
- [25] D. Bradley, P. Gaskell, X. Gu, Burning velocities, Markstein lengths, and flame quenching for spherical methane-air flames: a computational study, *Combust. Flame* 104 (1996) 176–198.
- [26] N. Otsu, A threshold selection method from gray-level histograms, *IEEE Trans. Syst. Sci. Cybernetics* 9 (1979) 62–66.
- [27] F. Weinberg, *Optics of flames*, Butterworths, 1963.
- [28] F. Williams, *Combustion theory: The fundamental theory of chemically reacting flow systems*, Combustion science and en-

- gineering series, Menlo Park, Calif. Benjamin/Cummings Pub. Co., 1985.
- [29] M. Matalon, B. Matkowsky, Flames as gasdynamic discontinuities, *J. Fluid Mech.* 124 (1982) 239–259.
 - [30] C. Wu, C. Law, On the determination of laminar flame speeds from stretched flames, *Symp. (Int.) Combust.* 20 (1984) 1941–1949.
 - [31] A. Kelley, J. Bechtold, C. Law, Premixed flame propagation in a confining vessel with weak pressure rise, *J. Fluid Mech.* 691 (2012) 26–51.
 - [32] F. Wu, W. Liang, Z. Chen, Y. Ju, C. Law, Uncertainty in stretch extrapolation of laminar flame speed from expanding spherical flames, *Proc. Combust. Inst.* 35 (2015) 663–670.
 - [33] H. Pitsch, FlameMaster: A C++ computer program for 0D combustion and 1D laminar flame calculations, 1998.
 - [34] J. Warnatz, N. Peters, B. Rogg, *Numerical Methods in Laminar Flame Propagation*, 1982.
 - [35] M. Smooke, Reduced kinetic mechanisms and asymptotic approximations of methane-air flames, volume 384 of *Lecture Notes in Physics*, Springer-Verlag, Berlin, 1991.
 - [36] F. Egolfopoulos, C. Law, Chain mechanisms in the overall reaction orders in laminar flame propagation, *Combust. Flame* 80 (1990) 7–16.